ROTATION AND SURFACE CHARACTERIZATION OF SPACE DEBRIS AND NEO TARGETS AT COMENIUS UNIVERSITY

M. Zigo, J. Šilha, D. Žilková, T. Hrobár, and P. Jevčák

Comenius University, 842 48 Bratislava, Slovakia, Email: M.Zigo, matej.zigo@fmph.uniba.sk

ABSTRACT

In the recent years, the space debris group with usage of the 70-centimeter reflector AGO70, operated by Comenius University in Bratislava, conducted extensive research in photometric characterization of space debris and near-Earth objects (NEOs). This research resulted in publicly available photometric catalogue of light curves, which contains folded rotational phase diagrams, estimated periods and parameters such as amplitude with related uncertainties. Such catalogue is a minimal requirement to perform more dedicated research and extensively describe the nature of the investigated targets.

Photometric light curves of rotating objects contain complex information about the object's shape and reflective properties. Amplitude of the detected signal is directly related to the physical properties of the object (size, albedo, shape, slope factor), mutual geometry between the sun-object-observer and attitude properties.

The BVRI photometry uses the folding of light curves in four different photometric passbands into the rotational phase diagrams to estimate the color index dependence along the rotational phase. This curve provides the initial information about the target's attitude and the low-resolution surface materials characterization. Target's position in the BVRI diagram is directly related to the most dominantly reflective materials and can be used for the material categorization.

In our work we present the overall strategy for the space object characterization, namely phase function and absolute magnitude extraction, rotation axis determination for cylindrical objects, and surface characterization through BVRI photometry and laboratory spectroscopy. Some of the developed methods will be applied also to NEA objects to demonstrate their applicability in this field.

Keywords: Photometry; Object characterisation; Rotational phase diagrams.

1. INTRODUCTION

The astronomy at Comenius University has a long tradition. Originally, the primary focus had been on astrometry and photometry of minor bodies of our solar system from meteoroids up to the asteroids. In recent years, the space debris group evolved with similar research methods, but focused mainly on the artificial objects. By definition, into this category belong all artificial objects on geocentric or other orbits, which lost or ended their mission i.e., non-functional satellites, spent rocket bodies and smaller fragments generated during the mission or by disintegration of more complex bodies. For the purposes of this article, we pinpoint three basic orbital regimes; Geo-synchronous orbits (GEO) with mean altitude $35,786$ kilometers, Geo-transfer orbit (GTO) with low perigee of hundreds of kilometers and apogees in the altitude of GEO ring. These orbits are subsets of High-elliptic orbits (HEO) which take place between the lowest regions up to the GEO ring. Mentioned will be also orbital regimes of Low-Earth orbits (LEO), between 250 and $2,000$ kilometers, which are at present most frequently utilized due to the cost-effective satellite release.

Thanks to the traditional astronomic methods, these objects can be observed, their orbit determined or improved and saved to catalogs. However, using the photometric follow-up observations, we can acquire many different useful information. They might help to reveal the true nature of the fragments creation mechanisms, link existing fragments back to their parent bodies, categorise objects according the similarities in their surface optical properties or add valuable information for active debris mission designs. Such motivations instigate the research of the Space Debris group at Comenius University.

The whole research started with the deployment of the new 70 centimeter aperture Newton reflector, which is, in its entirety owned and operated by the Comenius University and situated at University's Astronomical and Geophysical observatory in Modra. Detailed specifications are provided in Section 1.1. This instrument was in recent years upgraded to a LEO sensor, which is able to observe all targets with altitude higher than 600 kilometers.

The space debris group at Comenius University demonstrated sensor's tracking capabilities and astrometric ac-

curacy during different campaigns with different tasks [1]. However, in this study we are presenting groups ability to collect and analyse data for the sensitive photometric and spectroscopic object characterization purposes. Each method has its own section allocated. Section 2 discusses the approach for single channel light curve processing and apparent rotational phase function reconstruction as well as the formation of the Space Debris Light Curve Database [2].

Section 5 discusses the methodology, which can be used for the estimation of the parameters such as albedo, size, shape and slope factor using the target's absolute magnitude dependencies on the phase angle i.e, the phase curves. This analysis shall improve the categorization of the populations and bring additional physical properties to object characterisation.

Section 3 contains the definition and demonstration of the ability to estimate the object's tumbling axis direction for cylindrical bodies based on the signal's amplitude modeling. The overall rotational state of the target has to be known for the active debris removal mission planning. For future applications, the forces which can affect the rotational states has to be further investigated.

All of these methods can be applied to improve the information which can be derived from the multichannel photometry as BVRI photometry. This methodology is described in the Section 4. Such approach can provide initial attitude information, low-resolution map of the surface reflectance properties, but also shall be used for the definition of the material groups and categorization mechanism. In this section the general approach for the Photometric reduction and color index estimation is discussed.

The logic of our implementations is based on the knowledge acquired in the research of natural minor bodies of our Solar system, so they are directly applicable also on the data reduction of the NEO or other observations.

Additionally, the Comenius University operates own network of all-sky cameras (AMOS) [3] developed for the observation of the meteor events in the atmosphere. Along the main all-sky camera optical system, a spectral camera AMOS-Spec-HR is installed. These cameras are able to record the spectra of specular flashes of LEO satellites, which can be correlated with the databases of laboratory based measurements and used for more sensitive material recognition and material groups definition [3]. Such categorisation can be transferred into the BVRI photometric system or other methods as a reference system for data interpretation [4].

1.1. Instrumentation

Majority of data used for our research is originated in the 70 centimeter aperture Newton reflector (AGO70) (see Fig. 1 and Table 1). It is situated 30 km far from the Bratislava at Astronomical and Geophysical observation in Modra, Slovakia (AGO) of Comenius University and registered at Minor Planet Center observatory list with code M34 [5].

Figure 1. AGO70 newton telescope on fork equatorial mount inside of its dome at Astronomical and Geophysical observatory in Modra [2].

Table 1. AGO70 definition parameters [2]

Operator	FMPI
Telescope	AGO70
Telescope design	Newton
Mount	Equatorial (Open fork)
Camera	CCD FLI-ProLine KAF-1001E
Dimension	1024x1024
Primary Mirror [mm]	700
Focal length [mm]	2962.0
Focal ratio	f/4.2
FoV [arc-min]	28.5 x 28.5
iFoV [arc-sec/px]	1.67

This computerized scientific instrument is operated by the Faculty of Mathematics, Physics and Informatics (FMPI), Comenius University Bratislava. Its field of research is dedicated to the observation of the space debris and NEOs. AGO70 is able to track dominant part of objects' population with mean altitude above 800 km and perform the astrometric and photometric measurements. AGO70 has installed the filter-changing wheel in front of the CCD camera with Johnson/Cousin's photometric filters, which enables to perform all types of photometric measurements including the sensitive BVRI photometry. Installed photometric filters are B - blue, V -visible/green, R_c - red and I_c - near-infrared. The transmission of each passband is plotted in Fig. 2.

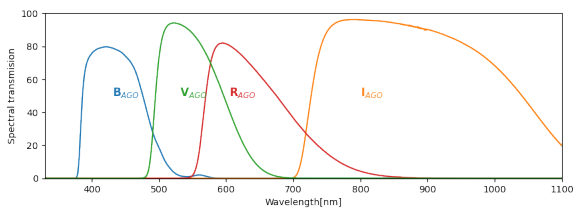

Figure 2. Transmission of the photometric filter set installed at AGO70.

2. PHOTOMETRY - APPARENT ROTATION ESTIMATION

The most crucial and established routine is the light curve processing. The routine starts with CCD images dark and flat calibration. Software AstroImageJ [6] is used for the image calibration and for the aperture photomery of the observed series. The aperture photometry uses the standard system of three concentric apertures, where from the first one is integrated the target signal, the second one is omitted to prevent the contamination with other frame objects and the third is used for integration of sky background intensity. Single point intensity is represented by subtraction of the sky intensity value is and object's intensity value. The measurements are sorted according to the time and light curve is constructed.

The next step is the rotational phase reconstruction and period estimation, which are performed using the Phase dispersion minimization [7]. This method is based on the comparison of light curve points time position to the set value of period. The main purpose of this method is to fine-tune the initial estimate of the rotational period and fold the light curve into the rotational phase diagram. The best solution corresponds to the minimal value of dispersion. If the value of period is close to the real value and no aliasing effects take place, the final phase diagram will be smooth curve without point clusters or scattered points. Afterwards, the phase diagram is approximated with Fourier series of the 8^{th} degree.

The general requirements on the data acquisition for this method is that the light curve shall last for at least one and half of the rotational period to be able to extract the period from the data. Otherwise, the light curve is considered as unprocessable or a slow rotator. Another requirement is for the data acquisition cadence to be slightly changed for some part of the light curve to avoid the aliasing effects.

Example of processed light curve of CZ-3B rocket body (COSPAR 2018-072C, Norad 43624) observed at 24^{th} March, 2022 is shown in Fig. 3 and its constructed phase diagram is shown in Fig. 4.

2.1. Space Debris Light Curve Database

The Space debris light curve database (SDLCD, www.sdlcd.space-debris.sk) [2] is publicly available database containing photometric measurement acquired using the AGO70. The database contains online searchable interface. The full non-public version of SDLCD contains in total more than 1800 tracks for about 400 individual objects (to date December 2022). All tracks are in arbitrary instrumental magnitude system i.e., not reduced to the standard system of magnitudes. More than 80% of the tracks show periodic signal and the apparent rotation period could be extracted and the rotation phase constructed [1]. The next data release is planned in Spring of 2023. For each reported series is provided the following information:

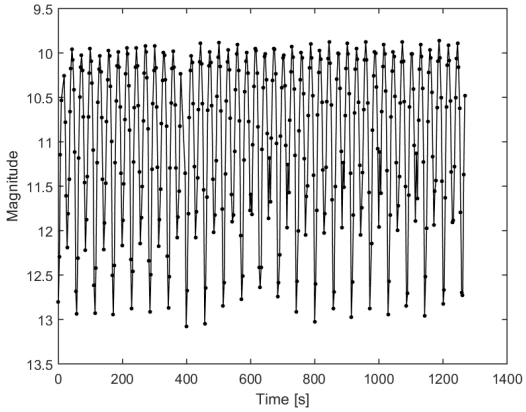

Figure 3. Light curve of CZ-3B rocket body (COSPAR 2018-072C, Norad 43624) acquired from observation with date at 24^{th} March, 2022.

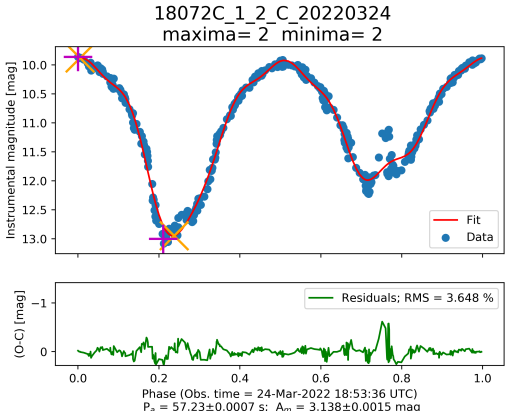

Figure 4. Phase diagram of CZ-3B rocket body (COSPAR 2018-072C, Norad 43624) acquired from light curve observed with date 24^{th} March, 2022.

- the title in format COSPAR_used observation filter_number of series_date of observation (yyyymmdd)
- reconstructed phase diagram with Fourier fit of 8th order
- residuals graph
- the light curve properties: source (raw light curve data also available), period [sec], period error [sec], ADU error, magnitude error, number of points, exposure [sec], APD (Average point distance) [sec], MedPD (Median distance between two measurement points in the light curve) [sec], ModePD (Moderate distance between two measurement points in the light curve) [sec], STDPD (Standard deviation of the point distance) [sec], Filter, AmpMath (mathematical amplitude calculated from the extremes of the Fourier function) [mag], AmpDat (measured amplitude of the light curve calculated as difference of the global extremes) [mag]. The list also contains error values.

- object and orbital properties: object name, object type, NORAD, orbital period [min], inclination [deg], perigee [km], apogee [km] and if the object decayed. All this data came from USSTRATCOM.

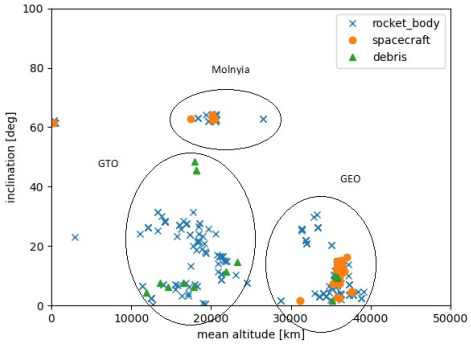

Figure 5. The mean altitude versus inclination distribution of the catalogued targets. Specific orbital regimes are marked and rocket bodies, spacecrafts and debris object are distinguished.

3. PHOTOMETRY - ATTITUDE DETERMINATION

The rotation axis orientation is calculated by using Williams model [8]. The model for rotation axis determination is suitable for cylindrical objects with reflective dominant mantle and non-reflective ends of cylinder, with rotation around the axis which is perpendicular to the central axis of object. It is based on calculation of difference between maximum and minimal value of object's brightness, the so-called brightness ratio, and its comparison with measured brightness ratio. The brightness ratio is function of satellite position, position of its rotation axis, and location of an observer. Location of the observer and the satellite position is known, also brightness ratio could be measured.

The brightness ratio is calculated for every possible tumble axis orientation. In the next step, tumble axis locations with calculated brightness ratio within +/- sigma of observed brightness ratio are chosen as possible solutions. This process is done for every observation of the object. Possible solutions, which are the same for every observation, are the most probable solutions and are shown in geocentric coordinate system. At least two observations with different phase angle are needed for successful calculation. The observations must be done within time the rotation axis orientation is not changed due to the natural effects. Solutions for possible directions of tumble axis of 2018-072C are shown in Fig. 6.

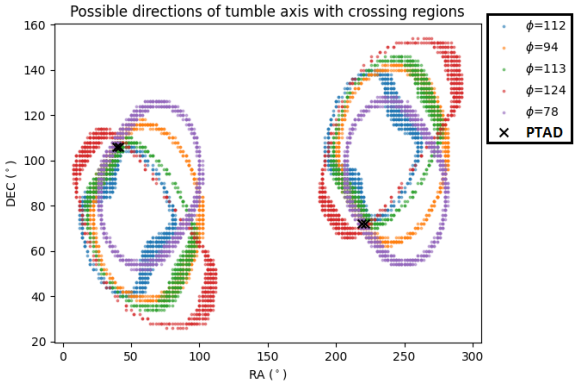

Figure 6. Possible tumble axis direction (PTAD) of 2018-072C calculated from data observed in June 2022.

4. BVRI PHOTOMETRY

In general the color photometry or BVR_cI_c photometry is a low-resolution spectroscopy, which is able to distinguish the target's surface materials regarding their reflection in different passbands of the visible light. For this purpose the term of color index is used, which represents difference between the measured light in two different channels and can be understood as a numerical expression of the target's surface color. It maps cumulative optical properties of target's surface.

Such method is also able to retrieve preliminary attitude information based on types of dominantly reflective materials [9], map the surface composition into the single materials [10], assess the affection by the space environment with rough estimates of the time spent on-orbit [11, 12] and correlate them with known populations into the material categories according to the similarities in the reflection [13].

FMPI implemented its own solution for the photometric reduction routine for the purposes of all-sky absolute photometry. It is utilizing the estimation of the first order extinction coefficient, which maps the intensity losses due the atmosphere and Zero-point and color transformation coefficient, which scale the instrumental system into the standard system of magnitude [14]. The photometric coefficients with related uncertainties are estimated using the standard solar analogs from the Landolt's catalog [15].

For the purpose of the BVR_cI_c photometry, each target is measured in all photometric passbands. The observation must be sensitively planned according to the type of object's orbital regime, angular velocity and pre-estimated apparent rotational period. During the observation, it must be ensured that the light curves in each channel will be evenly sampled, that at least one and half of the rotational period will be measured, and the phase angle will not change for more than 5 degrees during single filter wheel rotation. For example, for GTO target with rotation of approximately 90 seconds, such observa-

tion lasts for roughly 20 minutes with 1 second exposure and 70 points taken in each filter. AGO70 repeats the R_c filter at the beginning and the end of the series to check, whether the geometric condition did not change significantly during the observation.

All extracted light curves are transformed into the standard system of magnitudes using the valid solution from the photometric reduction for desired date of observation. If the target is stable non-rotating object, the average color indices are calculated and saved into the internal catalog. If it shows some periodic signal, the light curves are initially process using the routine described in Section 2. The time information is recorded respectively to the very first measurement in the series. The period estimation and phase dispersion minimization methods are done simultaneously for all passbands to ensure the accurate alignment of the reconstructed rotational phase functions in each filter. Afterwards, rotational phase functions are optimized by the Fourier series of 6^{th} degree, to obtain mathematical expression of the curve. Afterwards, color indices as function of the rotational phase are estimated.

Such approach enables to extract the color index rotational phase curve, which maps the color index variation along one rotational phase of our target. The color index rotational phase curve along with reconstructed rotational phase diagrams can be seen on Fig. 7.

The example on Fig. 7 shows the observation of the Falcon 9 rocket body. Its shape is approximately cylindrical with first half of highly reflective white-painted tank, bottom base with less reflective dark nozzle and reflective upper base. In this regard it can be expected that in the B-V versus R-I, it will appear near the sun's color indices, in the category III from categorization defined in [13]. Highly reflective targets belong to this category, which spectra is in average flat with some small discrepancies i.e., they reflect only the spectrum of sunlight. In case of higher amplitude, it is expected that in the recorded signal will repeat the signatures of the reflective tank, bottom nozzle and upper base.

On the bottom part of the Fig. 7 can be seen the color index phase curve with marked position of the signal's extremes by the crosses. The local extremes of the rotational phase diagram lie near the turning points of the color index rotational phase curve. As the maximal reflection is driven by the coat, it can be expected that the maxima will lie close together. Their separation is caused only by the small contribution of the materials from the partially visible bases. If we assume that the nozzle shall be affected by the burning of the fuel, it shall appear more dimmer (1^{st} minimum on Fig. 7) than the upper base (2^{nd} minimum on Fig. 7), which only held the carrier. Therefore, the color index is less affected by the reflection of the nozzle and closer to the color indices of the maxima. The width of the turning point is wider as the nozzle is composed of different materials. The more reflective upper base is further separated, but as the material of upper base is more homogeneous, the turning point is narrower.

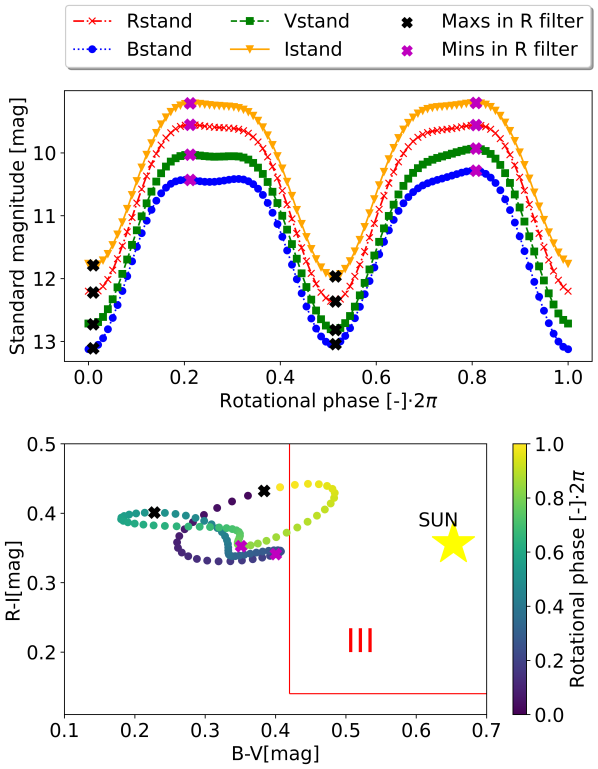

Figure 7. BVR_cI_c photometry result for the Falcon9 rocket body with COSPAR 2019-009C observed from AGO70 at 30^{th} of September 2019. On the upper image can be seen the rotational phase diagrams in all channels. The middle and bellow plots show the color index rotational phase curve with and without the material categories taken from [13]

If the shape of the investigated target is approximately known, such analysis can provide initial attitude information i.e., distinguish the reflection of the specific part of the body. For the more complex bodies as satellites or less cylindrical shaped upper stages, the curve is getting much more complex. But the material groups defined by work as [13] and [3] or other reference points in this diagram can help map, which part of the target is currently driving the reflection i.e., whether the solar panel or the MLI insulation of the body segment is mostly dominant.

5. PHOTOMETRY - PHASE CURVES

For phase functions of artificial objects, i.e., change of brightness as a function of phase angle, extensive research have been conducted by [16] where authors proposed to use for artificial objects a sphere as a first assumption. Two different reflectance properties were defined for the sphere, diffuse reflection defined via function $F_1(\phi)$ and specular reflection defined via $F_2(\phi)$. Their contribution in the resulting reflectance is defined via parameter β [-]. For the apparent magnitude of object

M_v [mag] defined has been following phase function:

$$M_v(\phi) = -2.5log(A\rho[\beta F_1(\phi) + (1-\beta)F_2(\phi)]) + 5log(R) - M_{sun} \quad (1)$$

where A [m^2] is mean cross-section, ρ is the geometric albedo, M_{sun} is the absolute magnitude of the Sun in photometric V filter, R is the range to object which is 1 AU expressed in meters, β=1 represents fully diffuse reflectance and β=0 represents fully specular reflectance. $M_v(\phi)$ for phase angle ϕ = 0° represents absolute magnitude, which could be also marked as H.

Obtaining observation points for the phase function analysis requires large effort. Data must cover longer period of phase angle values and for rotating or asymmetric objects different viewing angles must be secured for given phase angle geometry. During the preparation of this paper the data for the photometric phase curves were still being collected by the AGO70. However, for the demonstration purposes we here used for the analysis of phase function archive data obtained from MMT database [17] using observations data for two different radar calibration spheres, namely Calsphere 4 (65065H, 1520) and LCS 1 (65034C, 1361). In Fig. 8 and Fig. 9 are plotted reduced magnitudes (observed visual magnitudes corrected to 1 AU) as a function of phase angle for both objects for year 2022. Data were fitted with the Hejduk function where extracted were coefficients $A * \rho$ [m^2] and β.

For Calsphere 4 (A) we estimated for 2022 $A * \rho$ = 0.091±0.002 m^2 and β = 1.0±0.06, perfectly diffuse sphere. For LCS 1 we estimated for 2022 $A * \rho$ = 0.737±0.013 m^2 and β = 0.0±0.01, perfectly specular sphere. The diameter of Calsphere 4 (A) during launch was 0.3556 m (14 inch) [18], while diameter of LCS 1 was 1.12 m with corresponding mean cross Sections $A_{Calsphere}$ = 0.0993 m^2 and A_{LCS}=0.9985 m^2 respectively. By using the estimated parameters $A * \rho$ for each sphere, we can calculate geometric albedo for 2022 observations to be $\rho_{Calsphere}$ = 91.63±2.0% and ρ_{LCS} = 74.81±1.3%, respectively. For year 2017 (not plotted) we calculated $\rho_{Calsphere}$ = 93.63±1.0% and ρ_{LCS} = 75.61±0.4%. By comparing the values for both objects in 2017 and 2022, it seems that there was no noticeable change in the geometric albedo between investigated years.

6. NEO APPLICATION

All above mentioned methods and tools for the space debris research were adopted based on the already established and published methods from the asteroidal community. During the development of our routines was taken into account, that they shall be still applicable also on the observations of natural objects and dominantly the NEOs.

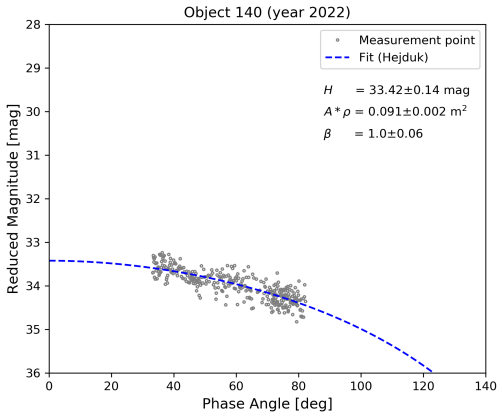

Figure 8. Reduced standard brightness of calibration sphere Calsphere 4 (65065H, 1520) observed with MMT system during year 2022 and the corresponding fit using Hejduk function.

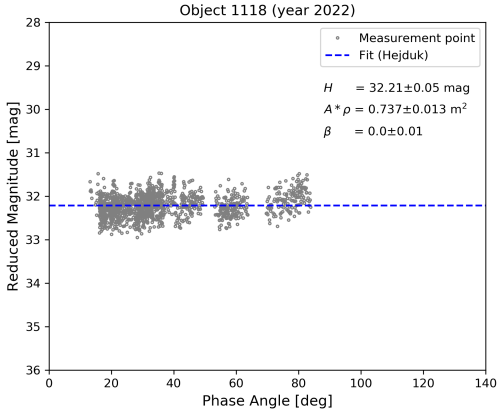

Figure 9. Reduced standard brightness of calibration sphere LCS 1 (65034C, 1361) observed with MMT system during year 2022 and the corresponding fit using Hejduk function.

AGO70 with its tracking capabilities described in Section 1.1 is able to track very close encounters of NEOs, with distances below 1 lunar distance. This provides the opportunity to investigate the NEO populations in wide scales of the distances and also to observe objects of smaller sizes and with rapid apparent rotation periods.

The observational strategies differ slightly according to the object's orbit, distance and rotational periods, but the methods as apparent rotational period estimation, phase curve construction and BVRI photometry can be directly used also for natural targets. This was partially demonstrated on the case of the asteroid 2018 CB observed during its close encounter at 9^{th} of February 2018 from AGO70. The object passed around the Earth in the distance of only 71000 kilometers and the observation lasted for approximately 3 hours. The apparent rotational period estimated from these data using methodology described in Section 2 was 321.355 seconds, which corresponds to

the values estimated and published by other authors [19]. The folded light curve into the rotational phase diagram can be seen in Fig. 10.

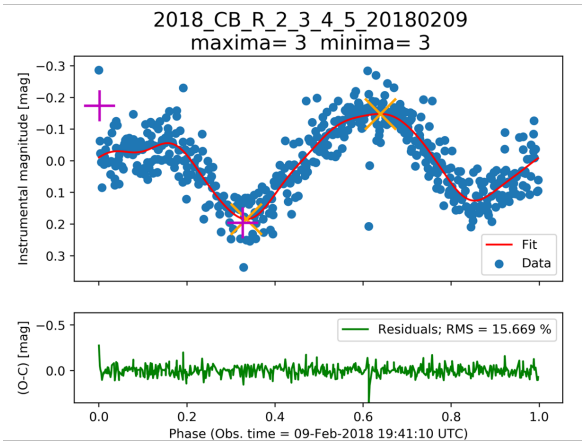

Figure 10. The folded light curve of the NEA target 2018 CB. Observations were conducted during night 9^{th} of February 2018 using AGO70. The estimated rotational period was 321.355 ± 0.18 *seconds. The amplitude of the measured signal was* 0.332 ± 0.003 *magnitudes. The asteroid was passing around the Earth in distance of* 71 000 *kilometers*

The application of our routines to the NEO targets help us validate our results and methods towards the already published works in this field. Such application brings also the opportunity for the cross-validation of the approaches, as the materials from the space engineering are commonly well described and their results can be in some cases, compared with the ground truth. This adds more reliability to the research and data interpretation on both sides. Besides of that, the albedo and color index catalogue can benefit from the addition of different targets' types to cover wide interval of reference materials for categorization and also in cases, when the nature of the target is completely unknown, as the return of distant artificial objects.

7. REFLECTANCE SPECTROSCOPY

Techniques of reflectance spectroscopy are already widely used in various fields of astronomy. This section investigates their application into space debris domain. A number of studies already examined reflectance spectra of in-orbit satellites and debris, specifically in Geosynchronous Earth Orbit (GEO) [13, 20, 21].

Initially, our focus was to identify primary types of very bright specular glints - reflections of sunlight from flat, shiny, highly-reflective surface elements. Such glints are regularly recorded by a system of spectral cameras AMOS-Spec-HR which are part of global AMOS network operated by the FMPI. AMOS-Spec-HR have holographic diffraction grating of 1000 $grooves/mm$ and spectral resolution of 0.5 $nm/pixel$ which after processing reduces to resolution of 1–2 nm at 1 micron [22].

Recorded reflectance spectra have the highest resolution in between 450-650 nm, hence this wavelength range is selected to best demonstrate the recorded data. Currently we operate with a database of more than 70 specular glints of LEO space debris and more are being recorded as the AMOS network expands world wide. So far 44 recordings had been processed and analysed, as summarized in Tab. 2.

Table 2. Summary of spectral types observed by AMOS-Spec-HR; spectral categories, their description and number of recorded spectra. [3]

Description	Category	No.
All spectra		44
Concave up shape	I	14
Increasing in red wavelengths	II	4
Flat, straight-lined	III	18
Cut-off or indeterminate		8

To process the data, spectral reduction techniques were adapted from lessons learned from asteroid spectroscopy and space debris ground-based observations [3]. Once processed, a clear pattern emanates within the data with some spectra being convex or with a concave up shape, others increasing towards regions of wavelengths corresponding to red colour, but mostly having the tendency to be flat or straight-lined. These three distinguished spectral types can be assigned into corresponding categories I, II and III, respectively.

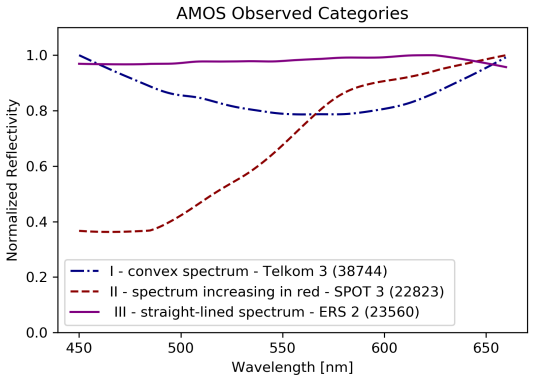

Figure 11. Three types of specular glints commonly recorded by AMOS spectral cameras; I – blue dot-dashed line – convex normalized spectrum of Telkom 3 (38744) satellite debris, II – red dashed line – increasing in red wavelengths, normalized spectrum of SPOT 3 (22823) defunct satellite, III – purple straight-lined normalized spectrum of ERS-2 (23560) defunct satellite. [3]

When considering specular glints, it can be assumed that the sunlight is mostly reflected from a sole type of dominant shiny surface element and hence the spectrum can be associated to a specific material generally used in satellite or spacecraft design. Common types of specular glints

recorded by AMOS-Spec-HR are illustrated in Fig. 11. To connect the distinguished categories with particular materials we have conducted a series of spectral measurements with AMOS-Spec-HR camera in a controlled laboratory environment. Measured were samples of the original DuPont Kapton polyimide foil, copper-coloured, and 30 nm thick aluminium foil which was on the other side of our Kapton sample. We have also measured the spectrum of Gallium arsenide multi junction solar cell supplied by a cooperating Slovakian company Needronix. Each of these normalized spectra, displayed in Fig. 12, can be assigned into one of the material categories determined from AMOS recorded data.

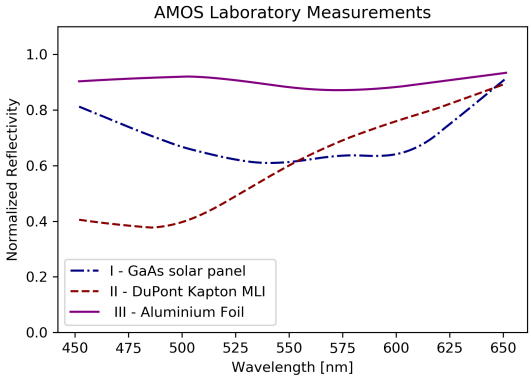

Figure 12. Laboratory measurements of specular glints of different materials commonly used in satellite design were conducted. Three different materials can be assigned into categories distinguished amidst AMOS-Spec-HR observational data; I – blue dot-dashed line – Gallium arsenide solar panel multi junction cell, II – red dashed line – DuPont Kapton multi-layer insulation foil (copper-coloured), III – purple straight-line – Aluminium foil with 30 nm thickness.

To conclude, from AMOS reflectance spectra, recorded either in a laboratory environment or during regular night-sky observation, three categories are distinguished. Material's or object's spectra measured can be assigned into each category as follows:

- **Category I:** GaAs solar cell, silicon solar cell, Telkom 3 satellite glint
- **Category II:** Kapton polyimide copper or golden coloured film (typical surface layer of Multi-Layer Insulation), copper foil, SPOT 3 satellite glint
- **Category III:** Aluminium and aluminium alloy foils, other silvery metals, white or black paint, ERS-2 satellite glint, Iridium flares

8. CONCLUSION

In this work were described different methods of the object characterization through the photometric and spectroscopic methods utilized at Comenius University. The AGO70 as primary instrument is focused on the observation of the space debris and NEO objects and estimation of their rotational characteristics and physical and optical properties.

We presented the general logic of the light curve processing towards the apparent rotational period estimation and general properties of our space debris light curve database. This method was also applied on the observation of the NEA 2018 CB and its apparent rotational period was estimated with accurate compliance with already publish results. AGO70 now continues with the building of the space debris light curve catalogue and increases the effort on the monitoring of the NEA close encounter events to expand the internal catalog also for the light curve of natural objects.

The attitude determination model based on the modeling of the brightness ratio under different phase angles was implemented for the cylindrical targets. This model provides the possible tumble axis direction, which can be used for the estimation of the more accurate characterization of the perspective under which the object was observe. The long-term monitoring of the objects help describing the processes and forces changing the direction of the tumbling axis, which is crucial to understand before the active debris removal can be utilized.

Observations performed in different photometric passband of the visible and near-infrared spectrum can be used for the material categorization of the targets. Through the construction of the color index phase curve, the BVRI photometry is able to acquire initial attitude information, distinguish different component of the object and correlate them with similar populations and material groups. The BVRI photometric routines will be further used for the monitoring of the aging and spaceweathering effects and for the construction of the color index catalog of the space debris and NEA objects.

We showed that from the phase curves i.e., phase angle dependence of the absolute magnitudes, the geometric albedo can be directly derived. This approach is demonstrated on the Calsphere 4 (65065H, 1520) test data from the MMT database. In the future AGO70's own data will be for this analysis used and the research will focus more on the individual object characterization and identification of its physical properties.

Furthermore, discussed were the spectroscopic observations conducted with AMOS all-sky cameras and processing of the recorded diffraction spectra. Acquired spectra were correlated with laboratory based measurements of selected material samples. Such observation can be used to investigate aging and space weathering effects on the objects surface properties and in the near future, the database of the reference materials shall be expanded for different samples for more accurate object characterization. As already mentioned, this characterization can be used for lower resolution methods as BVRI photometry.

ACKNOWLEDGMENTS

We acknowledge the support of staff contributing to the operation of the AMOS systems in Slovakia, and the Instituto de Astrofísica de Canarias for providing support with the operation of AMOS systems in Canary Islands. We also acknowledge the Department of Experimental Physics of Faculty of Mathematics, Physics and Informatics, Comenius University Bratislava, and Needronix s.r.o. for support with laboratory spectral measurements. This work was supported by the Comenius University Grant Žilková_UK/383/2022_FMFI and Zigo_UK/338/2021_FMFI and Zigo_UK/247/2020_FMFI.

REFERENCES

1. Šilha, J., Krajcovic, S., Zigo, P., Tóth, J., Zigo, M., Žilková, D., ... Flohrer, T. (2021). Development and operational status of AGO70 telescope. In Proceedings of the 8th European Conference on Space Debris, Darmstadt, Germany.
2. Silha, J., Krajcovic, S., Zigo, M., et al. (2020). Space debris observations with the Slovak AGO70 telescope: Astrometry and light curves. Advances in Space Research. doi: https://doi.org/10.1016/j.asr.2020.01.038.
3. Žilková, D., Šilha, J., Matlovič, P. et al. (2022). Space debris spectroscopy: specular reflections at leo regime. Advances in Space Research. doi:https://doi.org/10.1016/j.asr.2022.12.001.
4. Zigo, M., Žilková, D., Šilha, J., Matlovič, P., Tóth, J. (2021). Combined effort of reflectance spectroscopy and BVRI photometry in the field of space debris characterization. In Proceedings of 8th European Conference on Space Debris, ESA/ESOC, Darmstadt, Germany.
5. IAU, Minor Planet Center(2022). The international astronomical union minor planet center. URL: https://www.minorplanetcenter.net/iau/lists/ObsCodesF.html.
6. Karen A Collins, John F Kielkopf, Keivan G Stassun, and Frederic V Hessman. Astroimagej: image processing and photometric extraction for ultra-precise astronomical light curves. The Astronomical Journal, 153(2):77, 2017.
7. Stellingwerf, Robert F. "Period determination using phase dispersion minimization." The Astrophysical Journal 224 (1978): 953-960.
8. Williams, V. (1979). Location of the rotation axis of a tumbling cylindrical earth satellite by using visual observations: Part i: Theory. Planetary and Space Science, 27(6), 885-890.
9. Cordelli, E., Schlatter, P., Schildknecht, T. (2018). Simultaneous multi-filter photometric characterization of space debris at the swiss optical ground station and geodynamics observatory zimmerwald. In Advanced Maui Optical and Space Surveillance Technologies Conference (AMOS)
10. Rodriguez, H., Abercromby, K., Mulrooney, M. et al. (2007). Optical properties of Multi-Layered insulation. In Proceedings of Advanced Maui Optical and Space Surveillance Technologies Conference
11. Pearce, E. C., Weiner, B., Block, A. et al. (2019). Examining the effects of on-orbit aging of sl-12 rocket bodies using visible band spectra with the mmt telescope and 5-color photometry with the ukirt/wfcam. In Advanced Maui Optical and Space Surveillance Technologies Conference (p. 69).
12. Jorgensen, K., Africano, J., Hamada, K. et al. (2004). Physical properties of orbital debris from spectroscopic observations. Advances in Space Research, 34, 1021–1025. doi:10.1016/j.asr.2003.02.031
13. Vananti, A., Schildknecht, T., Krag, H. (2017). Reflectance spectroscopy characterization of space debris. Advances in space research, 59(10), 2488–2500
14. Zigo, M., Šilha, J, Hrobár, T., Jevčák, P., (2023) Space debris surface characterization through BVRI photometry, Advances in Space Research [In preparation]
15. Landolt, A. U. (2009). Ubvri photometric standard stars around the celestial equator: updates and additions. The Astronomical Journal, 137(5), 4186.
16. Hejduk, M., Specular and Diffuse Components in Spherical Satellite Photometric Modeling, Proceedings of AMOS Conference, held in Wailea, Maui, Hawaii, September 13-16, 2011, Edited by S. Ryan, The Maui Economic Development Board, 2011.
17. Karpov et al, "Massive photometry of low-altitude artificial satellites on Mini-Mega-TORTORA", Revista Mexicana de Astronomía y Astrofísica (Serie de Conferencias) Vol. 48, pp. 112-113 (2016).
18. NASA Space Science Data Coordinated Archive, https://nssdc.gsfc.nasa.gov/nmc/spacecraft/display.action?id=1965-065H, 2023.
19. Birtwhistle, P. (2018). Lightcurve Analysis for Four Near-Earth Asteroids. Minor Planet Bulletin, 45, 178-181.
20. Bédard, D., Wade, G., Jolley, A. (2014, September). Interpretation of spectrometric measurements of active geostationary satellites. In Proc. of the Advanced Maui Optical and Space Surveillance Technologies Conf (pp. 1-16).
21. Abercromby, K. J., Rapp, J., Bedard, D., Seitzer, P., Cardona, T., Cowardin, H., ... Lederer, S. (2013, April). Comparisons of a Constrained Least Squares Model versus Human-in-the-Loop for Spectral Unmixing to Determine Material Type of GEO Debris. In Sixth European Conference on Space Debris (No. JSC-CN-28507).
22. Matlovič, P., Tóth, J., Kornoš, L., Loehle, S. (2020). On the sodium enhancement in spectra of slow meteors and the origin of Na-rich meteoroids. Icarus, 347, 113817.